Revista Mexicana de Astronomía y Astrofísica, **27**, 213-218 (1993)

THE STAR–FORMATION HISTORY OF GR8 WITH HST IMAGERY

Ryan J. Wyatt and Reginald J. Dufour
Department of Space Physics and Astronomy, Rice University

RESUMEN

Se presentan resultados del estudio de imágenes de la galaxia irregular cercana GR8 obtenidas utilizando la "Wide Field Camera" del telescopio espacial Hubble. Estos datos nos permiten llevar a cabo la fotometría de estrellas hasta una magnitud $R \sim 24.5$ con resolucíon superior a las observaciones terrestres. Se presentan diagramas color-magnitud para los filtros "*BVR*" y son comparados con las trazas evolutivas de estrellas massivas con metalicidad muy baja. Concluímos que la historia de formacíon estelar de GR8 durante los últimos 10^9 años se llevó a cabo como una "onda" que viaja de NE a SO en la galaxia y no como un solo brote de formacíon estelar.

ABSTRACT

We report the results of a deep imaging study of the nearby irregular galaxy GR8 using the Wide-Field Camera on the Hubble Space Telescope. These data enable us to perform photometry on stars as faint as $R \sim 24.5$ with spatial resolution superior to ground-based observations. Color–magnitude diagrams in the "*BVR*" filters are presented and compared with cluster isochrones and evolutionary tracks for massive stars of very low metallicity. We conclude that the star formation history of GR8 during the past 10^9 years resembles a "wave" progressing from the NE to the SW parts of the galaxy, as opposed to a single starburst event.

Key words: **GALAXIES: IRREGULAR — GALAXIES: PHOTOMETRY — GALAXIES: STELLAR CONTENT**

1. INTRODUCTION

When Reaves (1956) discovered GR8 (DDO 155, A1256+14), he believed it to be a member of the Virgo cluster. However, subsequent studies (*i.e.*, Hodge 1967) placed it in the outer regions of the Local Group at a distance of approximately 1 Mpc. De Vaucouleurs & Moss 1983 derive a a distance modulus of $(m - M) = 25.25 \pm 0.4$ (corresponding to 1.1 Mpc), an isophotal diameter of 1.1′, and $M_B = -10.7$, placing GR8 among the least luminous of nearby star–forming galaxies. Hoessel & Danielson (1982) found a distance modulus of ~26.1 from G–R band CCD imagery using the KPNO 2.1–m telescope. More recent imagery puts its distance at 1.0 Mpc and confirms that it is an outlying member of the Local Group (Aparicio, Garcia–Pelayo & Moles 1988). VLA 21–cm maps suggest that the visible components of GR8 are embedded in an HI core of nearly uniform density surrounded by a "dark matter halo" (Carignan, Beaulieu & Freeman 1990), based on derived masses of M(stars) = $1.2\times10^6 M_\odot$ and M(HI) = $2.0\times10^6 M_\odot$ compared to the larger dynamical mass estimate of $3.9 \times 10^7 M_\odot$.

The most detailed Hα imaging study is by Hodge, Lee, & Kennicutt (1989), using CCD data obtained with the KPNO 2.1–m telescope. They identify 32 HII regions, most of which are small, have low surface brightness, and appear localized in the vicinity of individual O stars. Spectrophotometry of one of the brightest HII knots (Hodge's No. 2) by Skillman et al. (1988) indicates that O/H is only 3% solar in the ISM of GR8. This places GR8 in a small group of "super-metal-poor" star–forming galaxies (*i.e.*, having O/H$\leq$ 5% solar), which may be indicative of systems newly formed from the collisions of IGM HI clouds. Indeed, the mass and metallicity of GR8 bears greater resemblance to dwarf spheroidal systems than irregular (Im) or blue-compact

galaxies (BCGs), making it an exceptionally interesting candidate for detailed photometry that would allow determination of the age and evolutionary characteristics of its stellar population.

The Hubble Space Telescope (HST) offered the opportunity to provide deeper photometry with higher spatial resolution than any previous ground-based studies, and this paper is the result of a Cycle 1 program (GO2416) in which we undertook such a photometric study. In this paper, we present several color–magnitude diagrams (CMDs) of the entire galaxy as well as selected regions within the galaxy. Compared to corresponding ground-based observations, our photometry allows for much more substantial understanding of how star formation has proceeded in GR8.

2. OBSERVATIONS AND DATA REDUCTION

The HST Wide-Field Camera (WFC) imaged GR8 on 1991 July 13–14, using five wide-band and two narrow-band filters at a resolution of 0.1 arcseconds per pixel. The 2.6–arcminute square field encompasses the entire extent of the galaxy, which lies at the intersection of the four CCDs that constitute the image plane. The five wide-band images (see Table 1) form the basis of this study. Each image consists of two 1200–second exposures, paired for the removal of cosmic rays.

Data reduction followed the standard procedures for HST WF/PC images. We used the Space Telescope Science Data Analysis Software (STSDAS) *calwfp* routine to perform analog-to-digital (A-to-D), bias, pre-flash, dark, and flat-field corrections on the raw images with a calibration data set received in 1992 March (see Table 2). The flat-field data available at that time did not include flats for F555W, F702W, or F785LP: the available exposures through those filters used F122M as a neutral-density filter, so we derived the F122M signature from the F502N and F622W flats, which had exposures taken through both the single filters and the filters plus F122M. For example, dividing the F502N+F122M flat field by the F502N flat field, we arrived at an approximation to the F122M signature appropriate for the F555W images. The technique worked best on the F555W image compared to the F702W or F785LP images; however, we succeeded in removing the filter and OTA signatures in all three frames.

Finally, two "CR–split" exposures through each filter allowed us to combine the images using the standard anti-correlation option in the STSDAS *combine* function. Only one pair of exposures (F785LP) required alignment before using the cross-correlation algorithm.

Table 1. — HST exposures of GR8, giving filters and exposure times.

Filter Name	Number of Exposures	Exposure Length	Date
F336W	two	1200	1991 July 13
F439W	two	1700	1991 July 13
F555W	two	1200	1991 July 13
F702W	two	1200	1991 July 14
F785LP	two	1200	1991 July 14

Table 2. — Calibration files used in image processing.

File Type	File Names	Filter(s)	Flat Field Names
DQF	bb615191w.r0h	F336W	c1d1031jw.r6h
		F439W	c191513cw.r6h
A-to-D	c2614032w.r1h	F502N	c191513gw.r6h
		F502N+F122M	c1d1456aw.r6h
Bias	bb61518rw.r2h	F555W	c191513jw.r6h
		F622W	c191513nw.r6h
Pre-flash	bb615194w.r3h	F622W+F122M	.r6h
		F702W	.r6h
Dark	bb61518tw.r5h	F785LP	c1915143w.r6h

3. PHOTOMETRY AND CALIBRATION

We performed the stellar photometry in an automated fashion, employing IRAF's *apphot* aperture-photometry package for all our measurements. We used *daofind* to locate prospective stars in all four frames through each filter. Images through the F555W, F702W, and F785LP filters provided many more detections than F336W and F439W imagery; thus, our deepest CMDs are not V vs. $(B-V)$. We then performed small-aperture photometry on the sources detected by *daofind*: an aperture 1.5 (0.15″) pixels in radius was used to measure the contribution from the source, while a sky value was estimated by taking the modal value of data in an annulus with inner radius 3.0 pixels and outer radius 6.0 pixels.

We chose small apertures for our calculations based on the success of the method demonstrated by Gilmozzi *et al.* (1990). Approximately 15% of the light in the HST point-spread function (PSF) is concentrated in a small (less than 0.1″, or one-pixel) "core," with the remaining light spread out in a complex halo covering several tens of pixels. Although the "core-aperture photometry" technique uses only $\sim$ 15% of the detected light, it nonetheless gives us high-resolution photometry of stars in GR8 that were unresolved in previous, ground-based studies.

We further cross-correlated the positions of stars detected through each of the five filters to come up with a list of magnitudes and colors for confirmed stars: if an object was detected by *daofind* and its flux measured with reasonable accuracy by the IRAF *apphot* package through more than one filter, then it is included in our CMDs. Again, the increased sensitivity of the HST CCDs at longer wavelengths gave us many more detections on the F555W, F702W, and F785LP images than on the others. The $(B-V)$ diagram in particular includes only the brightest stars in our sample (with $V < 23$), whereas the "$(V-R)$" and "$(V-I)$" diagrams go much deeper—*i.e.*, $R \approx 24.5$.

After arriving at relative magnitudes from our photometry, we used the aperture corrections in the Wide Field/Planetary Camera Final Orbital/Science Verification Report, Chapter 12, to adjust our numbers to the standard HST values.

Finally, for stars detected through both the F336W and F439W filters, we used the relationships in Harris et al. (1991) to convert from the HST filter set to Johnson–Morgan magnitudes. The Harris equations offer an easy and straightforward conversion from F439W and F555W to B and V (*n.b.* Equations 2 and 3):

$$(\mathrm{F336W}-U) = +0.0769(U-B)+0.0176(U-B)^2-0.114 \quad (1)$$

$$(\mathrm{F439W}-B) = -0.0915(B-V)+0.0168(B-V)^2 \quad (2)$$

$$(\mathrm{F555W}-V) = +0.0768(B-V)-0.0254(B-V)^2 \quad (3)$$

$$(\mathrm{F702W}-R) = -0.1526(V-I)-0.0055(V-I)^2 \quad (4)$$

$$(\mathrm{F785LP}-I) = -0.0549(V-I)-0.0343(V-I)^2 \quad (5)$$

However, transformations from other HST filters to Johnson–Morgan values require knowledge of the colors in more than two filters, so we could not transform the data without sacrificing the depth of our imagery. Therefore, all other CMDs are presented in the HST filter magnitudes—*i.e.*, we plot F555W vs. (F555W − F702W) in lieu of V vs. $(V-R)$.

4. RESULTS

We divided GR8 into three regions that include most of the galaxy's brightest stars. Region 1, in the SW, contains the bluest stars in GR8 and corresponds to the "HL5" Hα complex in Hodge et al. Region 2, in the central part of the galaxy, includes the brightest stars and corresponds to "HL19" in Hodge et al. Finally, Region 3 contains a "V"-shaped group of prominent stars (*e.g.*, numbers 4, 10, 14, and 16 in de Vaucouleurs & Moss 1983) in the NE part of the galaxy. In addition, we have defined two regions that exclude stars included in the first three regions. Region A includes stars within approximately a half-arcminute of the center of GR8 that do not fall inside regions 1, 2, or 3, and region B consists of stars not within the other four.

Fig. 1 presents CMDs in V vs. $(B-V)$ for the entire galaxy and regions 1 and 2. Evolutionary tracks for 40-$M_\odot$, 25-$M_\odot$, 20-$M_\odot$, and 15-$M_\odot$ stars with metallicity $Z = 0.002$ appear as solid lines in Fig. 1(a), and the dotted line represents an interpolated main sequence. Both the evolutionary tracks and the main sequence are adapted from Maeder (1990) using color tables from the Yale Revised Isochrones (Green, Demarque & King

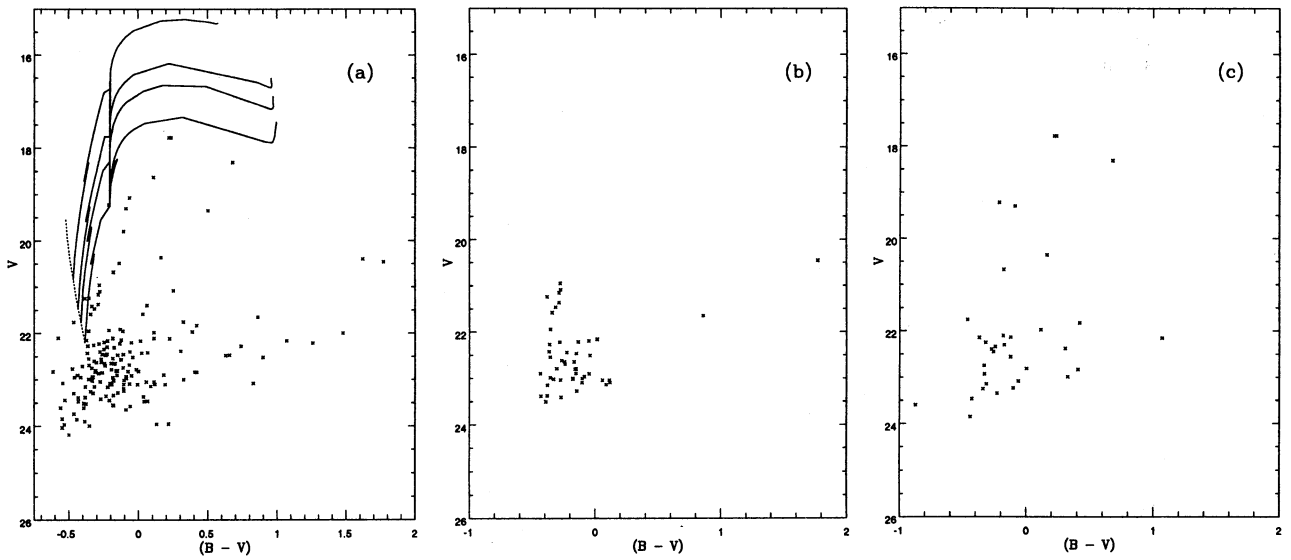

Fig.1. — V vs. $(B-V)$ photometry of GR8, for the entire galaxy in (a), region 1 in (b), and region 2 in (c). Evolutionary tracks from Maeder 1990 are overplotted in (a) for $40M_{\odot}$, $25M_{\odot}$, $20M_{\odot}$, and $15M_{\odot}$ as solid lines and a Zero-Age Main Sequence as a dotted line.

1987) to convert to V and $(B-V)$. Compared to the entire galaxy in Fig. 1(a) and region 2 in Fig. 1(c), region 1 in Fig. 1(b) shows the tightest grouping on the diagram, with a bright yellow star at $V \simeq 21.5$ indicating a turn-off at approximately $M_V \simeq -3.5$ for an assumed distance modulus of $(m-M) = 25.0$.

Fig. 2 presents CMDs in F555W vs. (F555W – F702W). Fig. 2(a) shows photometry for all stars identified in both F555W and F702W, with isochrones ($Z = 0.0006$) from the Yale Isochrones representing ages of 200, 500, 1000, 3000, and 10000 million years, again at an assumed distance modulus of $(m-M) = 25.0$. Regions 1 and 2 in Fig. 2(b) and 2(c) show structure similar structure to that seen in Fig. 1(b) and 1(c), as well as an underlying red population that appears even more pronounced in the CMD for region 3, as seen in Fig. 2(d). Although region B, shown in Fig. 2(f), covers ten times the area of region A in Fig. 2(e), less than a third as many stars appear in its CMD, indicating that the underlying red stars are a part of GR8 and not a foreground population.

5. DISCUSSION

Limited space precludes a detail discussion of the CMD fitting analysis currently in progress, but several characteristics of the stellar population and the history of star formation in GR8 are evident from Figs. 1 and 2. We further note the paper by Patterson, Wyatt & Dufour (1993) in this volume, for which the UV–optical imagery results for regions 1 and 2 suggest that the two brightest stars in region 2 (HL19) are likely foreground objects. In addition, the very low metallicity of GR8 makes detailed interpretation of the CMDs within the context of most published stellar evolution modeling and cluster isochrones inappropriate.

From Figs. 1 and 2 it is apparent that the brightest stars in GR8 are evolved B and A stars, rather than red supergiants or O stars, with $-0.2 < B-V < +0.2$. The brightest "red" stars are four stars with $(V, B-V) \approx (+20.5, +1.7)$, corresponding to supergiants of spectral type K, for which $M_V \sim -4.5$ (Mihalas & Binney 1981) and consistent with a distance modulus of $(m-M) = 25.0$. Such a distance modulus is further consistent with the brightest blue stars being $V \sim 19$—corresponding to $M_V \sim -6$, a value close to B or A supergiants in the Galaxy.

Assuming a distance modulus of 25.0 and the evolutionary tracks of Maeder (1990) for $Z = 0.002$ on the BV CMDs of Fig. 1, we derive ages for regions 1 and 2 of 15 and 40 million years, respectively. While not shown, the BV CMD for region 3 suggests an age of about 75 million years, but it shows a less obvious evolutionary track indicative of a well-defined star formation episode. Indeed, if one compares the various VR CMDs of

Fig. 2, it is apparant that the relative numbers of red to blue stars increase systematically going from regions 1 to 2 to 3 to A, indicating that we are looking at systematically older groups of stars in the selected regions. Regions 3, A, and B all show significant numbers of red stars with $(V, B-V) \sim (+24, +1.2)$ corresponding to the evolutionary tracks for metal-poor clusters of 200–500 million years (from Green et al.) for $(m-M) = 25.0$.

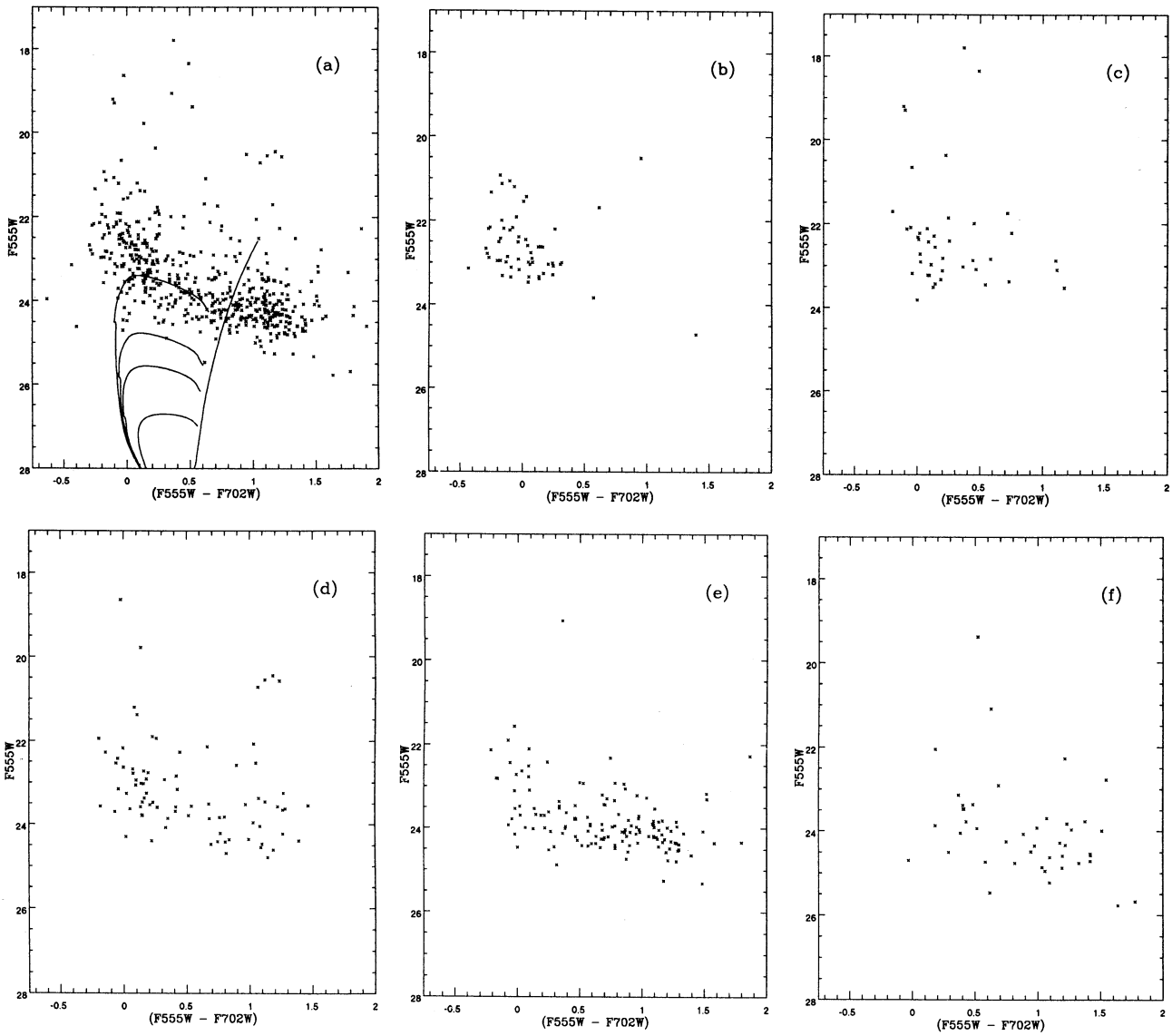

Fig. 2. — F555W vs. (F555W – F702W) photometry of GR8, for the entire galaxy in (a), region 1 in (b), region 2 in (c), region 3 in (d), region A in (e), and region B in (f).
Isochrones are overplotted in (a) for ages of 200, 500, 1000, 3000, and 10000 million years.

Nevertheless, the *BVR* CMDs suggest that the star–formation history of GR8 is not consistent with a single burst: at least three distinguishable recent (< 100 million-year) episodes are evident, as well as a surrounding older stellar population in the main body of the galaxy outside of the blue star associations and possibly farther out as well (we have not yet ruled out foreground stars at the $V \sim 24.0$ level here). We further note that regions 1, 2, and 3 all show HI concentrations from the study of Carignan et al., while no HI concentrations are seen elswhere (*i.e.*, region A in the main body and the perimeter region B).

Therefore, we conclude that GR8 has experienced a "wave"—rather than a "burst"—of star formation during the past billion years, with the earliest star formation occurring in the NE parts of the galaxy that is currently devoid of HI, more recent star formation in the N and S extremities of the main body where HI clouds are still present, and the most recent star formation on the SW edge of the galaxy where an HI cloud is also seen.

This research is supported in part by AURA grant GO–2416.01–87A for the Cycle 1 General Observer Program.

REFERENCES

Aparicio, A., Garcia–Pelayo, J.M., & Moles, M. 1988, A&AS, 74, 375
Carignan, C., Beaulieu, S., & Freeman, K.C. 1990, AJ, 99, 178
de Vaucouleurs, G., & Moss, C. 1983, ApJ, 271, 123
Green, E.M., Demarque, P., & King, C.R. 1987, *Revised Yale Isochrones and Luminosity Functions*, New Haven, Connecticut: Yale Univ. Observatory
Harris, H.C., Baum, W.A., Hunter, D.A., & Kreidl, T.J. 1991, AJ, 101, 677
Hodge, P.W. 1967, ApJ, 148, 719
Hodge, P.W., Lee, M.G., & Kennicutt, R.C. 1989, PASP, 101, 640
Hoessel, J.G., & Danielson, G.E. 1982, ApJ, 271, 65
Maeder, A. 1990, A&AS, 84, 139
Mihalas, D., & Binney, J. 1981, *Galactic Astronomy: Structure and Kinematics*, New York: W.H. Freeman and Co.
Patterson, B.R., Wyatt, R.J., & Dufour, R.J. 1993, RMexAA, this issue
Reaves, G. 1956, AJ, 61, 69
Skillman, E.D., Melnick, J., Terlevich, R., & Moles, M. 1988, A&A, 198, 33

Reginald J. Dufour and Ryan J. Wyatt: Rice University, Space Physics & Astronomy Dept., P.O. Box 1892, SS Bldg., Rm. 232, Houston, TX 77251-1892, U.S.A.